Received: 20 March 2020 | Revised: 27 April 2020 | Accepted: 11 May 2020

DOI: 10.1002/oa.2881

RESEARCH ARTICLE

The third dimension in palaeopathology: How can three-dimensional imaging by computed tomography bring an added value to retrospective diagnosis?

Hélène Coqueugniot[1,2,3] | Bruno Dutailly[1,4] | Olivier Dutour[1,2,5]

[1]UMR 5199 PACEA, CNRS/University of Bordeaux/Ministry of Culture, Pessac, France

[2]Chaire d'Anthropologie biologique Paul Broca, EPHE-PSL University, Paris, France

[3]Department of Human Evolution, Max Plank Institute for Evolutionary Anthropology, Leipzig, Germany

[4]UMS 3657 Archeovision, CNRS/University of Bordeaux Montaigne/University of Bordeaux, Pessac, France

[5]Department of Anthropology, Canada Social Science Centre, Western University, London, ON, Canada

Correspondence
Hélène Coqueugniot, UMR 5199 PACEA, CNRS/University of Bordeaux/Ministry of Culture, Allée Geoffroy Saint-Hilaire 33615 Pessac, France.
Email: helene.coqueugniot@u-bordeaux.fr

Funding information
Cluster of Excellence in Archaeological Sciences in Bordeaux, Grant/Award Number: ANR-10-LABX-52; Nouvelle-Aquitaine Regional Council; French-Russian Laboratory (CNRS/RAS), Grant/Award Number: LIA K1812

Abstract

Three-dimensional (3D) imaging is now extensively used for studying ancient human and animal bones. This method has been consensually adopted by palaeoanthropologists, but its interest in palaeopathology has been challenged. The aim of this paper is to illustrate the contribution of 3D reconstructions to retrospective diagnosis in palaeopathology. We selected six palaeopathological cases among our research corpus representing three nosographic categories (trauma, infection and neoplasia) from various periods ranging from the Middle Palaeolithic to the beginning of the Modern Era. For each case, we compared the diagnostic value of plain X-ray, computed tomography (CT) slices, and 3D reconstructions. The latter were performed using TIVMI program, a free software for research use developed by one of us. Reconstructions are obtained by surface extraction that follows a segmentation process. We showed that this 3D method allowed reconstructing/quantifying pathological processes on ancient bones, usefully supplementing conventional radiological analyses and clearly bringing an added value to retrospective diagnosis in palaeopathology.

KEYWORDS

3D reconstruction, CT scan, palaeoimaging, palaeoradiology, surface extraction

1 | INTRODUCTION

The application of radiological methods to bioarchaeology is contemporary with the birth of palaeopathology, as a new scientific term. Only 3 years after Shufeldt's note coining this term (Shufeldt, 1893) and a few months after the description of this new electromagnetic radiation by the German physicist Wilhem Röntgen (Thomson, 1896), the first radiographs of Egyptian mummies were performed at the Vienna Museum of Natural History (Dedekind, 1896) and at the Senckenberg Museum in Frankfurt (König, 1896), concomitantly with the development of its medical applications (Béclère, 1898; Rowland, 1896).

If Ruffer, who firstly defined palaeopathology as an autonomous science (Ruffer, 1913), did not mention the interest of X-ray exploration while he developed many other analytical methods on Egyptian mummies (Ruffer, 1921), the use of radiology in bone palaeopathology would have been promoted shortly afterwards by palaeopathologists and physicians (Baudouin, 1923; Moodie, 1923; Pales, 1929). A short time later, Moodie published his monograph entirely devoted to the radiographic study of Egyptian and Peruvian mummies

(Moodie, 1931). He illustrated by abundant iconography the decisive use of radiology in anthropological determination, palaeopathological diagnosis and recognition of animal species in mummy studies, allowing the archaeologists to study the contents without altering the container. As a flip side, Moodie already pointed out the image superimposition (projection on the same plane), as a limit in visualizing different structures crossed by X-rays. Despite this disadvantage, conventional radiology continues to provide, after more than a century, many services to palaeopathology (Mays, 2008).

Computed tomography (CT), which was introduced in medical field in 1971, solved this challenging issue of superimposition, in both clinical sciences and bioarchaeology. This technique was applied to mummy studies 6 years later (Lewin & Harwood-Nash, 1977) and 4 years after to palaeopathology (Wong, 1981). Since these pioneering works, many publications exploited the advantages of CT scanning to explore bioarchaeological issues. However, for some specialists in medical imaging, most of these publications suffered from weaknesses on research design, CT protocols and interpretative skills of nonradiologist authors (O'Brien, Battista, Romagnoli, & Chhem, 2009). Guidelines for appropriate settings of scanning and image reconstruction parameters were recently provided for CT scanning bioarchaeological material such as mummies (Panzer, Ketterl, Bicker, Schoske, & Nerlich, 2019).

Digital revolution initiated in the 1980s allowed a considerable development of X-ray acquisition and image processing, including three-dimensional (3D) reconstructions. As early as 1985, Conroy and Vannier predicted that 3D imaging could greatly help future palaeoanthropological research, allowing fossils to be visualized and analysed in a totally innovative way (Conroy & Vannier, 1985). This prediction has proven to be accurate, going further with the development of a new approach, called virtual (palaeo)anthropology (Weber, 2001). Specialists of human evolution almost unanimously recognized that 3D imaging has revolutionized their research, contrasting with the debate on 3D CT in palaeopathology. Indeed, since the first 3D reconstruction of a mummy face by (Marx & D'Auria, 1988) hailed as a "tour de force," the number of publications using 3D reconstructions applied to mummy sciences and palaeopathology increased rapidly (e.g. for mummy studies and palaeopathology; Allam, Thompson, Wann, Miyamoto, & Thomas, 2009; Appelboom & Struyven, 1999; Gostner, Pernter, Bonatti, Graefen, & Zink, 2011; Jansen, Poulus, Taconis, & Stoker, 2002; Lynnerup, 2008; Panzer et al., 2019; Pernter, Gostner, Vigl, & Rühli, 2007; Pickering, Conces, Braunstein, & Yurco, 1990; Wade et al., 2019) and for bone palaeopathology (e.g. Belcastro et al., 2014; Castro et al., 2019; Chamel, Coqueugniot, Dutour, Mindaoui, & Le Mort, 2017; Coutinho Nogueira et al., 2019; Flohr et al., 2015; Hernandez & Hudson, 2015; Plischuk, De Feo, & Desántolo, 2018; Richards, Ojeda, Jabbour, Ibarra, & Horton, 2013; Woo, Lee, Hu, & Hwang, 2015; Zuckerman, Garofalo, Frohlich, & Ortner, 2014). Faced with this craze, some authors (Chhem, 2006; Chhem & Brothwell, 2008) strongly advised against the use of 3D for palaeopathological research.

The aim of our paper is to bring additional arguments in this debate, showing that, when using appropriate methodology for 3D reconstructions, systematic comparisons between 2D and 3D imaging showed that 3D reconstructions can clearly provide an added value to the palaeopathological diagnosis.

2 | MATERIAL AND METHODS

2.1 | Material

The material consists in six palaeopathological cases, of infectious, traumatic or neoplastic origins and from periods ranging from prehistoric to historic times (Table 1), that we have previously analysed and diagnosed according to classical criteria used in palaeopathology (Buikstra, 2019).

We have selected these cases among our corpus of data, to exemplify the main situations in which the 3D approach can enrich the palaeopathological diagnosis, in addition to the two-dimensional (2D) imaging approach.

2.2 | Methods

To objectify the added value of 3D imaging to palaeopathological diagnosis, we reappraised each case by interpreting images from conventional 2D methods (plain X-rays and CT scan slices). When plain X-rays were not available, we digitally reconstructed them from CT acquisition, using an algorithm for flattening the voxel grid (see Supporting Information).

We performed 3D reconstructions from CT acquisitions for each of the selected cases. CT scan slices were open from DICOM format on a software dedicated to visualization and 3D reconstructions, which have been developed in our laboratory (Dutailly, Coqueugniot, Desbarats, Gueorguieva, & Synave, 2009). TIVMI® software (Treatment and Increased Vision for Medical Imaging) presents at least three advantages compared with other software programs based on marching cubes algorithms, which can alternatively be used in this approach: firstly, it is based upon the half-maximum height (HMH) algorithm developed by Spoor, Zonneveld, and Macho (1993) extended to 3D (Dutailly et al., 2009), which provides a higher level of precision in volumetric reconstructions than marching cubes method and minimizes the interobserver error (Guyomarc'h et al., 2012); secondly, it can be easily augmented with specific plug-ins; finally, it is freely downloadable (http://projets.pacea.u-bordeaux.fr/TIVMI/). The protocol we used for 3D reconstruction is based upon a surface extraction performed after manual segmentation process by greyscale thresholding, a method previously applied on mummies for palaeopathological purposes (Lynnerup, 2008; Pickering et al., 1990). We used two main approaches for segmenting anatomical or pathological bone organization: filling of emptied spaces and separating structures of different density. If a move of segmented elements is required, for instance, to replace fractured pieces in their anatomical position, other software such as Geomagic® or 3ds Max® have to be used.

TABLE 1 Studied cases presented in function of their chronology, bone topography, nosography, with original references

Case number	Site, specimen, chronological frame	Bone	Nosography	Original reference
1	Qafzeh, Israel adolescent individual 11, Middle Palaeolithic,	Skull	Traumatic	Vandermeersch, (1981), Dastugue, (1981), Tillier (1999)
2	Saint-Martial of Angouleme, France, adult female, Middle Age	Thoracic spine	Infectious	Anonymous (1975)
3	Iboussières, France, adult male, Upper Palaeolithic	Coxal/sacrum	Infectious	Dutour, Pálfi, Panuel, and Gély (1995), Aymard et al. (2007)
4	Saint-Come Priory, Middle Age (12th cent.), elderly male, France	Skull	Neoplastic	Dufaÿ and Gaultier (2011)
5	Saint-Laurent de Grenoble, Modern period (18th cent.), adult, France	Femur	Infectious	Colardelle, (1996), Hervieu, Herrscher, and Colardelle (2008)
6	Kaliningrad, Contemporary period (1812), young male, Russian Federation	Femur	War trauma	Buzhilova, Rigeade, Shvedchikova, Ardagna, and Dutour (2009); Dutour and Buzhilova (2013)

The details of our protocol are given in Supporting Information (Methods S1).

We compared the results of interpretation of 2D imaging with those we obtained by 3D imaging, in order to assess the respective contributions of these three imaging methods to the palaeopathological diagnosis. Our team has the main knowledge and skills required for interpreting radiological images, according to leading guidelines (van der Gijp et al., 2014).

3 | RESULTS

- Case 1: Endocranial reconstruction evidenced traumatic brain injury during Middle Palaeolithic.

Individual Qafzeh 11 (Middle Palaeolithic, Israel), an adolescent around 13 years old (Tillier, 1999; Vandermeersch, 1981), presents a lesion on the right side of the frontal bone, characterized by a

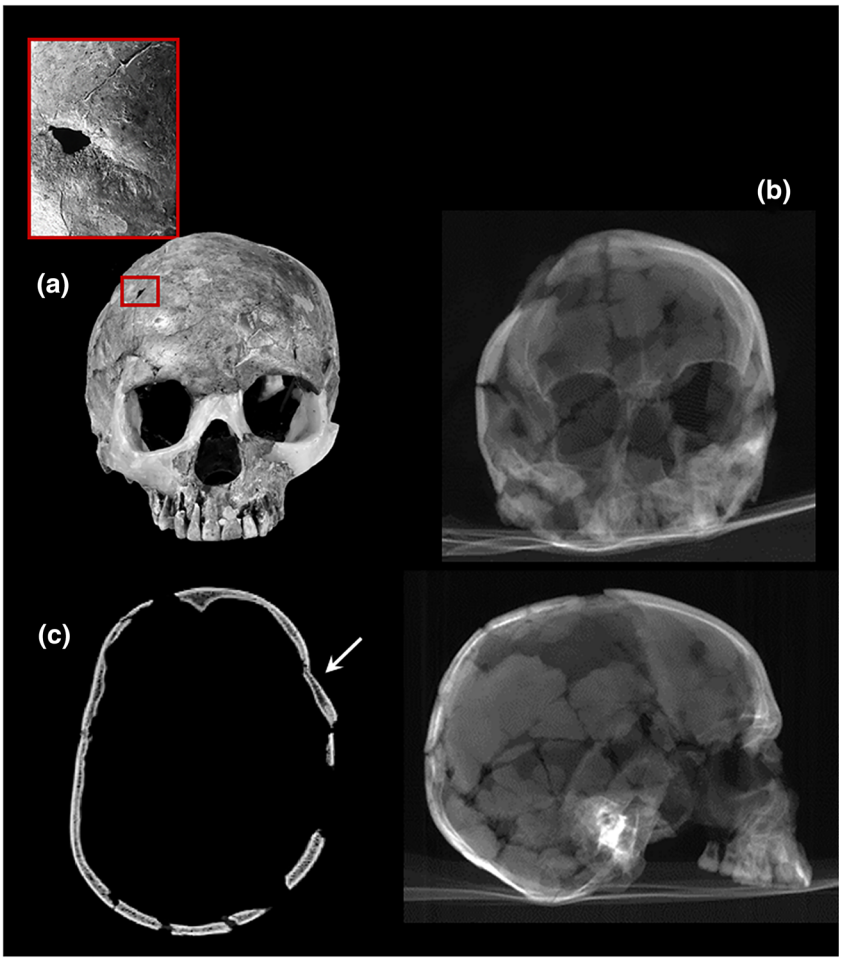

FIGURE 1 Skull of Qafzeh 11 (Middle Palaeolithic, Israel). (a) Morphological aspect with a focus on cranial lesion (right part of frontal bone). (b) Plain X-ray, frontal and right lateral views. Owing to the fragmentation and superimposition, the fracture line is not visible. (c) Computed tomography (CT) scan axial slice at the lesion level (arrow). A displacement of a fragment of frontal bone is visible, but the fragmentation of the skull and the restoration after its discovery do not formally rule out a taphonomic cause to this aspect [Colour figure can be viewed at wileyonlinelibrary.com]

depressed line that ends to up to an oval-shaped hole (Figure 1a) that was recognized since the discovery. Plain X-ray picture of the skull of this young individual was available (Tillier, 1999): besides the taphonomic fragmentation, the defect can be detected on the profile picture but does not provide any additional information (Figure 1b). On some of the CT sections, a displacement of a frontal fragment is observed, but it is impossible to determine whether if its origin is pathological or taphonomic (Figure 1c, arrow). The macroscopic, radiological and CT scan studies lead to the conclusion that this young individual experienced a fracture of the cranial vault, qualified as benign, and healed with no functional consequences (Dastugue, 1981).

More recently, a 3D reconstruction was performed (Coqueugniot et al., 2014). It used the firstly quoted approach (filling the emptied space, Figure 2a) in order to reconstruct the endocranial cast, which has been presented using transparency setting (Figure 2b). This procedure revealed additional information about the frontal trauma that is little (or not) visible using conventional morphoscopic and radiological methods. The frontal fracture was actually compound: the broken part of the frontal squama is depressed in its anterior part, penetrating inside the skull and responsible for intracranial depression and irregularities on the surface of the endocranial cast. In the posterior part of the frontal scale, the coronal suture is disengaged and lifted outward, revealing a diastasis of the suture (Figure 2c). The 3D reconstruction therefore reveals a depressed fracture of the frontal bone associated with brain damage. The diagnosis performed in 3D is therefore not a benign fracture but a severe traumatic brain injury (TBI).

- Case 2: Spinal canal reconstruction showed diameter preservation in Medieval Pott case.

Among the 40 burials discovered in Saint-Martial medieval cemetery of Angoulême (Anonymous, 1975), the skeleton of an adult female has drawn the attention of archaeologists. It presented a typical form of tuberculous spondylodiscitis (Pott's disease): eight thoracic vertebrae fused in a thoracic block, with a very acute angle apex at the level of T7, of about 100°. Owing to the associated ankyloses of the costovertebral joints, most of the ribs are attached to the spinal block (Figure 3a). In such a typical case, imaging is not useful for palaeopathological diagnosis, which is evident here, but the question is whether the medullar canal has been significantly narrowed by the cuneiform collapse. Indeed, this narrowing of the osseous spinal canal is one of the causes of Pott's paraplegia or paraparesis, besides other mechanisms of distension and compression of spinal cord (cold abscess, inflammatory tissue, sequestrum, etc.). These are not visible on dry bones, but paralysis of lower limbs due to vertebral collapse can be deduced from the thinning of their cortical bone (Marcsik,

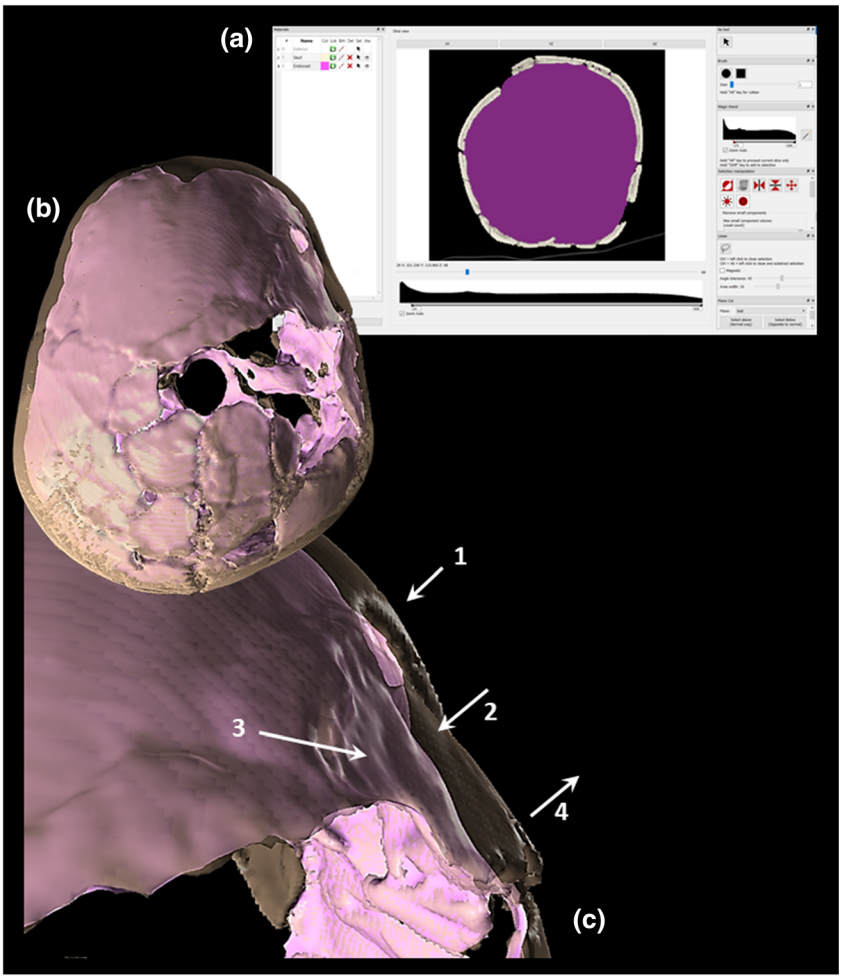

FIGURE 2 Three-dimensional (3D) reconstruction of Qafzeh 11 traumatic brain injury. (a) TIVMI software interface showing the virtual filling of the endocranial cavity in sagittal view. (b) 3D reconstruction in upper view (the skull vault appears in transparency and the virtual endocranial cast in pink). (c) Close-up view of the trauma area. 1, fracture line; 2, anterior part of the frontal bone depressed fracture penetrating the endocranial volume; 3, irregular shape of virtual endocranial surface indicating brain damage; 4, diastasis of the right coronal suture with an outwards bone projection due to the trauma [Colour figure can be viewed at wileyonlinelibrary.com]

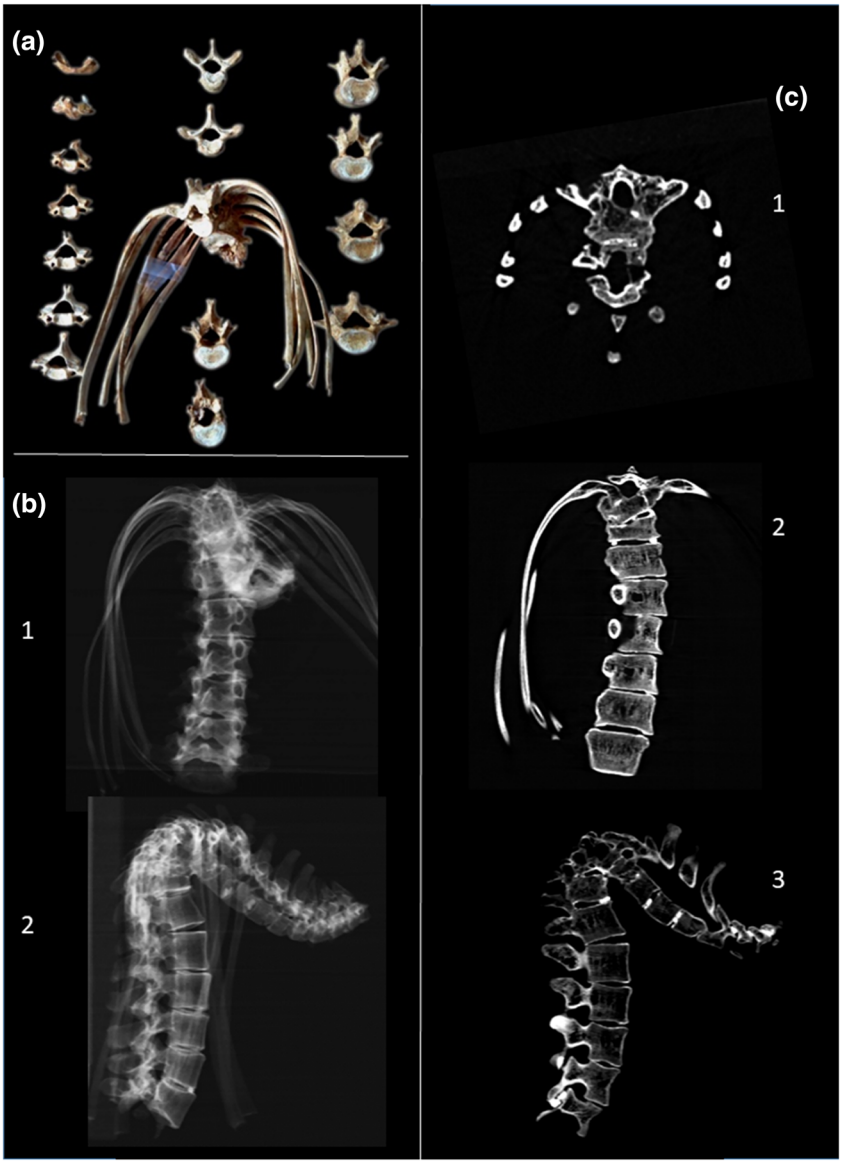

FIGURE 3 Medieval Pott's disease (Saint-Martial cemetery, Angoulême, France). (a) Morphological aspect. (b) Plain X-ray. 1, frontal; 2, lateral views showing the typical angular kyphosis, pathognomonic of Pott's disease, with a very acute angle, raising the issue of a possible Pott's paraplegia. (c) Computed tomography (CT) scan slices. 1, axial; 2, frontal; 3, sagittal planes. Owing to the strong angulation in both frontal and sagittal planes, the spinal canal morphology cannot be evidenced, whatever the slicing plane [Colour figure can be viewed at wileyonlinelibrary.com]

Szentgyorgyi, Gyetvai, Finnegan, & Pálfi, 1999). If these bones are missing, the narrowing of the spinal canal is a criterion to assess the issue of possible Pott's paralysis in palaeopathology.

Radiographs (Figure 3b) are not informative on the lesion, owing to the superimposition of ribs. The degree of kyphosis makes the interpretation of the CT scan slices difficult, whatever the orientation of the slice plane (Figure 3c): the diameter of the spinal canal along the vertebral block and at the angulation level is not accessible.

On the contrary, thanks to the virtual filling method (Figure 4a), the shape and size of the spinal canal become perfectly visible (Coqueugniot, Dutailly, Desbarats, Buzhilova, & Dutour, 2015). In our case, at the level of the angular kyphosis, the diameter of the spinal canal presents almost no narrowing: the anteroposterior diameter is indeed of 14.6 mm at the top of the angle in T7, whereas it measures 14.8 mm above (T3). These values are in the normal range of thoracic spinal canal anteroposterior diameter (Figure 4b and c).

- Case 3: Reconstruction of sacroiliac cystic cavities illustrated infectious pathways and mechanism at the end of Upper Palaeolithic.

Individual A from the Iboussières cave, Malataverne (Upper Palaeolithic, Drôme, France), is a mature adult presenting a left sacroiliac partial fusion (Aymard et al., 2007; Dutour et al., 1995) (Figure 5a). Plain X-ray confirmed the partial fusion of the left sacroiliac joint and revealed a rounded radiolucent image located on the joint area and surrounded by a thin line of sclerosis (Figure 5b). CT scan slices evidenced a central cystic-shaped cavity with well-defined and sclerotic borders, mainly developed on the ilium side; in addition, a posterior smaller cavity is identified (Figure 5c) developed on both the sacrum and ilium sides. However, the spatial relationships between these lesions and the sacroiliac joint are not easy to interpret on CT slices only. At this step, the hypothesis of infectious sacroiliitis, possibly of tubercular origin, can be proposed, but the aspect resulting

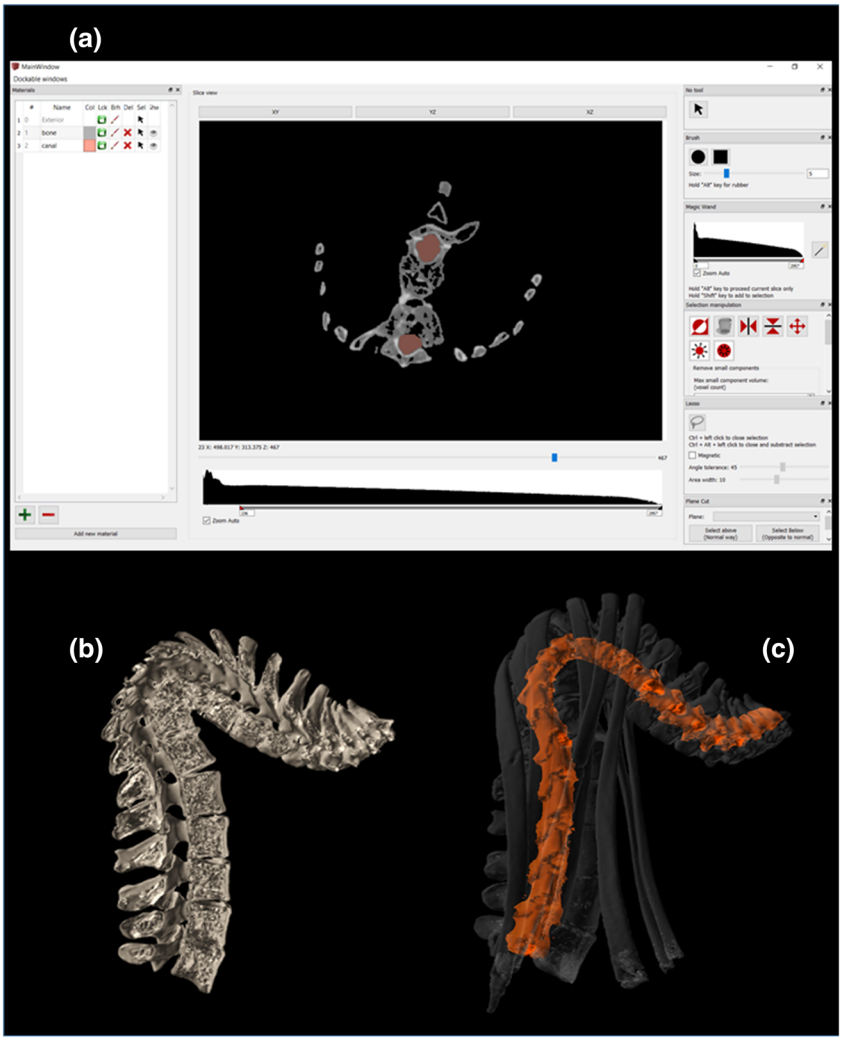

FIGURE 4 Three-dimensional (3D) reconstruction of Pott's disease. (a) TIVMI software interface showing the virtual filling of the spinal canal. (b) 3D virtual sagittal section showing the typical vertebral destruction with severe angular kyphosis. (c) 3D reconstruction of the spinal canal (orange) showing that, despite the severity of the angular kyphosis, the diameter of the spinal canal is not significantly narrowed, a fact that can be confirmed by measurements [Colour figure can be viewed at wileyonlinelibrary.com]

from the infection (two cystic cavities) and its process of spread remains unclear.

Then, the two cysts and the remaining space of the sacroiliac joint were segmented slice by slice, virtually filled and virtually extracted outside of the bone. This 3D reconstruction makes the relationships between these three structures clearly visible (Figure 5d): the two cysts appeared to be in mirror image and are not connected (8 mm apart for the closest distance). They are both well defined and poly-lobulated. The anterior cyst, more developed on the iliac side, is the largest (4.5 cm^3) and has no direct relationship to the remains of the sacroiliac joint; the posterior cyst is more than half as small (1.9 cm^3) and mainly extended on the sacrum side; it is in direct connection with sacroiliac joint in its rear part. This passage to the outside may correspond to the externalization of a cold abscess in the gluteal region (Figure 5e). Then the scenario could have been the following: the infection occurred by the haematogenic route on either bone of the sacroiliac joint and developed into a focal osteomyelitis, and then it reached the sacroiliac joint and the other bone; the healing process partially fused the joint, dividing the granulomatous osteomyelitis into two cysts. The anterior one was isolated, and the posterior was open on the sacroiliac joint that could have been responsible of a cold abscess in the gluteal area (Coqueugniot, Dutailly, Desbarats, Buzhilova, et al., 2015).

- Case 4: Reconstruction of lytic lesions on medieval skull allowed to quantify tumour volume.

Among the burials excavated in the Medieval Priory of Saint-Cosme (France), a skeleton of an elderly male came from a burial (F791) dated from the end of the 13th century (Dufaÿ & Gaultier, 2011). It presents multiple lytic lesions on the whole skeleton, including the skull (Figure 6a). These lytic lesions are clearly visible on plain X-ray (Figure 6b) and CT scan slices (Figure 6c), leading the diagnostic discussion to two main aetiologies: multiple myeloma and metastatic cancer (Dutour, Gaultier, Dufaÿ, Dutailly, & Coqueugniot, 2013). The distinction between these two pathologies is a challenge for the palaeopathologist, because even if differentiation criteria have been proposed (Rothschild, Hershkovitz, & Dutour, 1998), it may be difficult in some cases to exclude one of the two diagnoses to affirm the other, on the mere analysis of the cranial lesions. Indeed, the criterion of size regularity in lytic lesions, which is classically presented as being characteristic of multiple myeloma, is

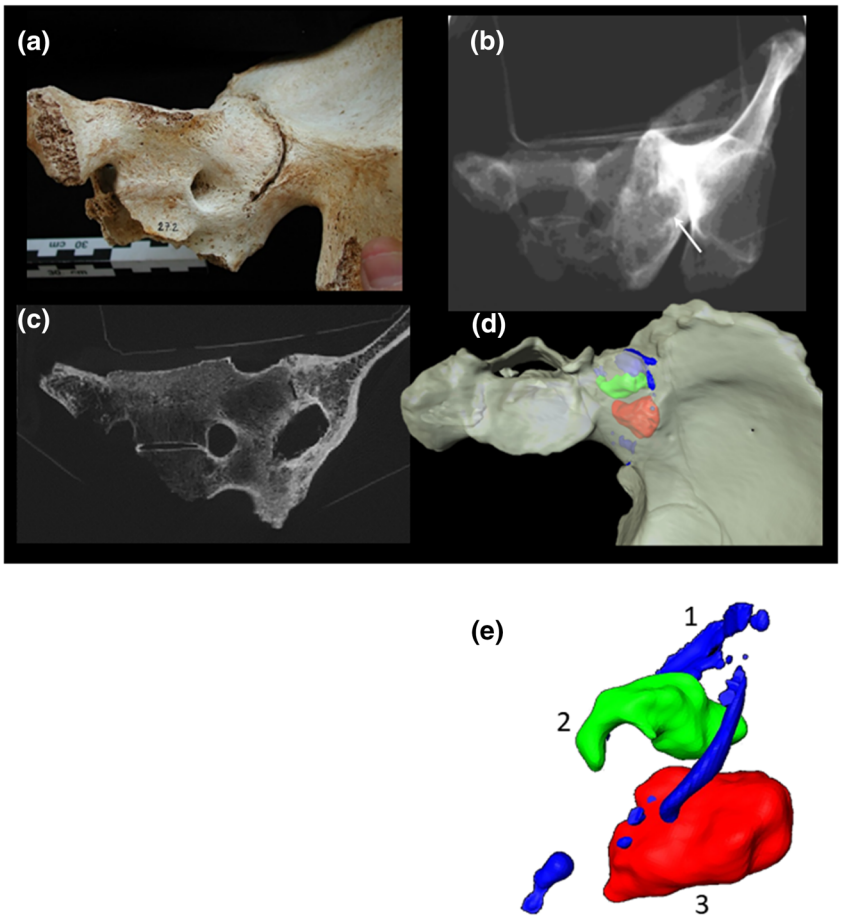

FIGURE 5 Sacroiliac fusion (Upper Palaeolithic, south-eastern France). (a) Morphological aspect. (b) Plain X-ray. Owing to superimposition, a rounded radiolucency is hardly visible (arrow). (c) CT scan, frontal slice. A central cystic-shaped cavity surrounded by sclerotic border is clearly visible (arrow). (d) Three-dimensional (3D) reconstruction of the sacroiliac fusion (upper view) showing in transparency two cysts (red and green) overlapping the sacroiliac joint (its remnants are identified in dark blue). (e) Virtual demolding of remnants of sacroiliac joint space (1) and the two cyst endocasts (2, posterior; and 3, anterior cysts). Contrary to the anterior cyst (red), the posterior one (green) is in direct communication with the posterior part of sacroiliac joint, allowing a possible constitution of a cold abscess inside the soft tissues of the lumbo-gluteal area [Colour figure can be viewed at wileyonlinelibrary.com]

not reliable because some lytic lesions of multiple myeloma can fused together, resulting in lytic lesions with different sizes, and reversely some metastatic cancers can result as well in lytic lesions of uniform size (Rothschild et al., 1998). However, it is not in the differential diagnosis that the interest of 3D lies in this case but in the possibility of approaching the evolutionary stage of a cancer by estimating the tumour mass, which is a unique situation in palaeopathology.

Indeed, the segmentation of pathological cavities (Figure 6d) makes it possible to quantify their volume: the software calculates the volume from the number of voxels contained in the segmented cavity and the volume of a voxel, which is known from CT scan acquisition data (Figure 6e). The sum of the volumes of the tumour cavities relative to the total bone volume will provide the percentage of the relative volume occupied by the tumour process, reflecting its mass. In our case, the average tumour volume for the entire skeleton is more than 16%. This is the first attempt in palaeopathology to quantify tumour volume from CT scan, which is a promising approach in clinical oncology, currently under development (Gaonkar et al., 2015). This 3D approach shows its superiority over 2D imaging in prognosis and follow-up in clinical oncology (Cai & Hong, 2018). Owing to this recent development, clinical tumour volume referential is not yet available for bone tumours, including multiple myeloma or metastatic cancer. However, it seems that in our case, the volume occupied by the tumour was sufficiently evolved to generate anaemia by bone marrow invasion and to be, among other tumorous mechanisms, at the origin of the death of this elderly man.

- Case 5: Reconstruction of femoral periosteal reaction illustrated gummatous osteoperiostitis during the early modern period.

In Grenoble (France), the excavation of the Priory of Saint-Laurent, which started in 1978, provided more than 1,500 graves dating from the 4th to early 18th century (Colardelle, 1996). Besides individual burials, some of the skeletons come from funeral vaults (Hervieu et al., 2008). Vault S 929, which was in use from the 15th to 17th century, provided several pathological cases, identified on intermingled bones; some of them showed alterations attributed to infectious origin, suggesting a diagnosis of osteomyelitis.

Among the long bones concerned, belonging to different individuals, a right femur is of interest because it presents a swelling at midshaft (Figure 7a), which is an unusual topography for osteomyelitis.

Plain X-ray revealed that the swelling is mainly due to a thickening of the subperiosteal cortical bone with few lacunae (Figure 7b); CT slices confirmed the predominant role of the periosteal reaction in the new bone formation as well as the moderate remodelling of the endosteal area (Figure 7c). This is more in favour of osteoperiostitis.

Diaphyseal bone and subperiosteal reaction were differentiated by manual segmentation on each CT slice, based on grey levels

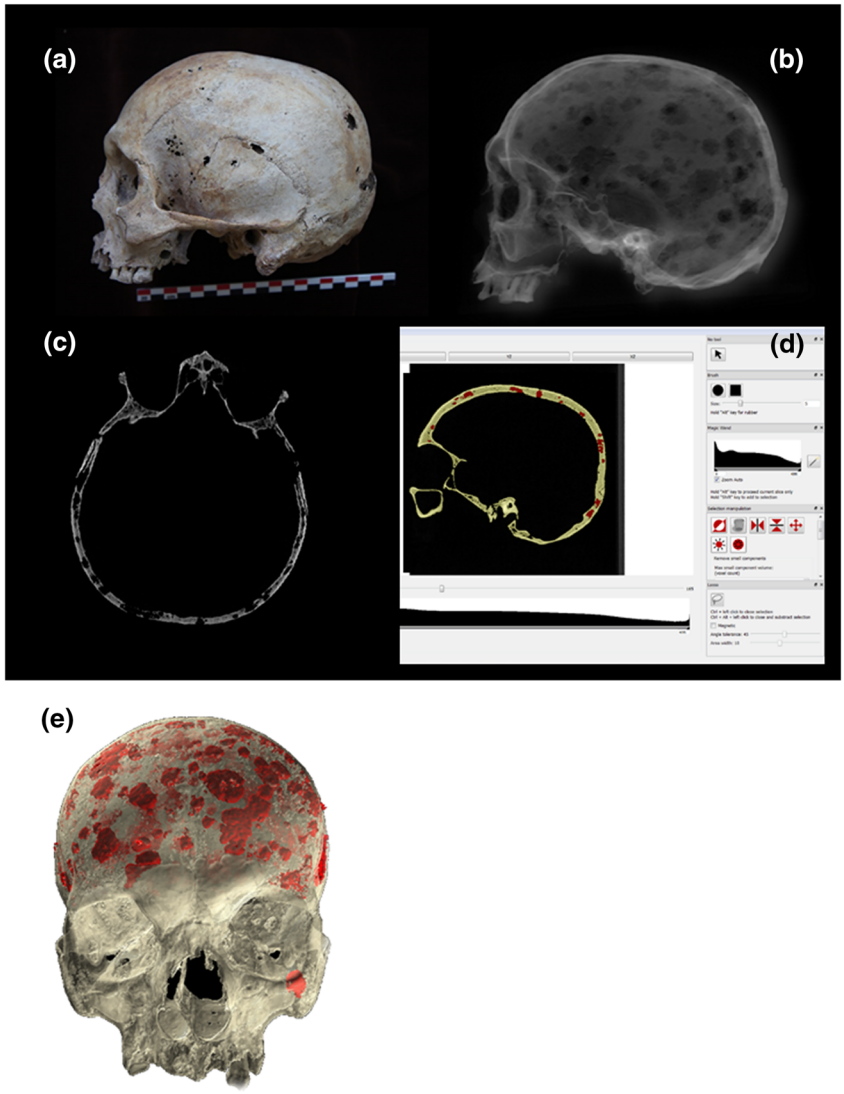

FIGURE 6 Lytic lesions on a medieval skull (Priory of Saint-Cosme, France). (a) Morphological aspect. (b) Plain X-ray lateral view showing multiple lytic lesions in favour of neoplasia (metastatic carcinoma or multiple myeloma). (c) Computed tomography (CT) scan, axial slice, showing the diploic origin of lytic lesions. (d) TIVMI software interface showing the virtual filling of each lytic lesions. (e) Three-dimensional (3D) reconstruction: besides the clear visualization of the neoplastic process, the quantification of its volume can be calculated [Colour figure can be viewed at wileyonlinelibrary.com]

corresponding to bone density. This step cannot be automated because it requires anatomical expertise on slices where the demarcation between normal bone and subperiosteal reaction is not very obvious. This process allowed us to obtain separate 3D reconstructions of the femoral diaphysis and the subperiosteal reaction (Figure 7d and e). It provided information about the aspect and volume of the pathological bone tissue and the prepathological state of the femoral diaphysis.

The subperiosteal reaction, which is mainly developed on the anterior and medial part of the femoral shaft, corresponds to a bone volumetric gain of 7% of the total diaphysis volume. The aspect of the lesion is clearly similar to the gummatous osteoperiostitis, which is typical of a treponemal infection (Hackett, 1976). The 3D reconstruction is not decisive for the diagnosis here, but it is the only way to approach the "prepathological state" and to quantify the development of subperiosteal new bone formation.

- Case 6: Reconstruction of femoral complex fracture evidence gunshot trauma during Napoleonic Wars.

In downtown Kaliningrad (Russian Federation), emergency excavations were conducted in Summer 2006 by a team of the Department of preventive archaeology (Institute of Archaeology, Russian Academy of Sciences). Twelve mass graves containing the remains of at least 600 individuals were discovered; skeletons were associated with military buttons, remains of textile, shakos, shoes, boots and coins that led to identifying these remains as those of Napoleonic soldiers of the *Grande Armée* (Buzhilova et al., 2009). This archaeological and anthropological material was studied in the framework of French-Russian Laboratory (LIA K1812, CNRS-RAS/EPHE-Moscow State University). The skeletal remains of soldiers revealed 103 evidence of war trauma including fractures and weapon wounds and evidence of war surgery such as amputations (Dutour & Buzhilova, 2013). Among these cases, the individual 6 from Pit E1, a young male of about 18 years old, exhibits a complicated trauma of the left femora. A callus had partly consolidated the fracture in bad position, with an internal angulation of about 135° (Figure 8a). The plain radiograph confirmed the fracturing of the femoral diaphysis into

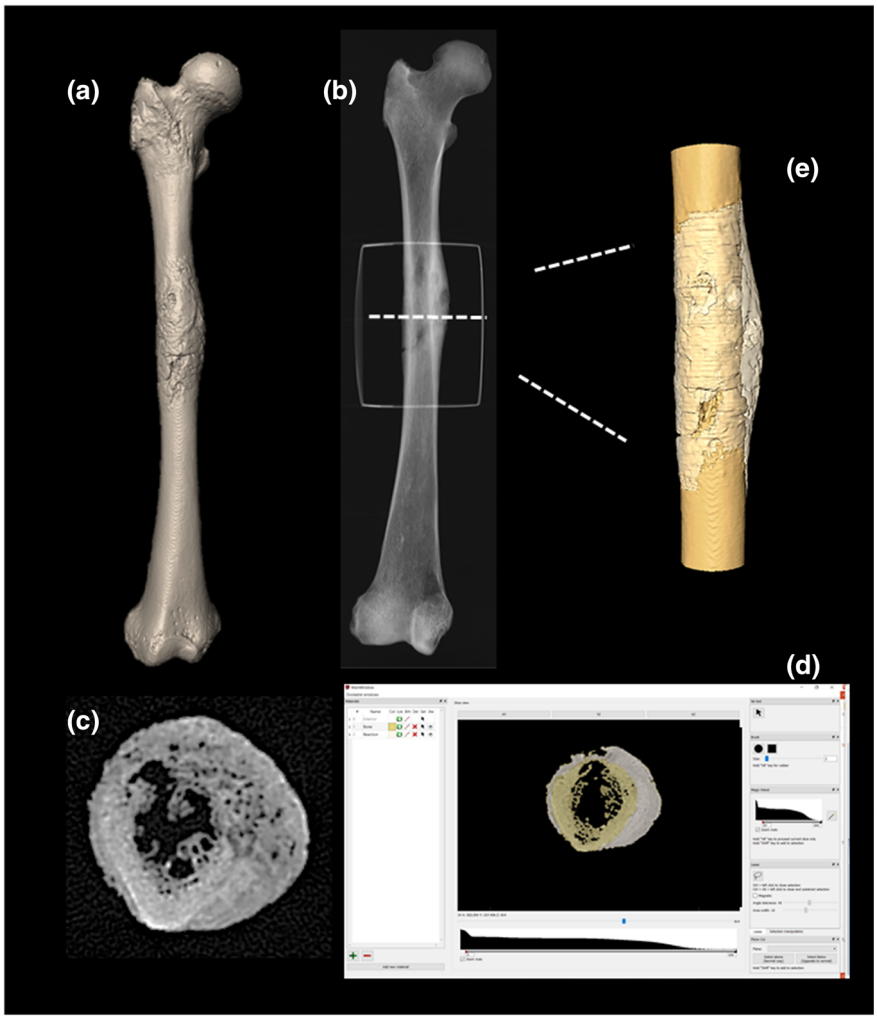

FIGURE 7 Femoral periosteal reaction (Priory of Saint-Laurent, Grenoble, France, 15th–17th century). (a) Morphological aspect showing a swelling at midshaft. (b) Plain X-ray revealing a thickening of the subperiosteal cortical bone with few lacunae. (c) Computed tomography (CT) scan, axial slice, evidencing the periosteal reaction at the origin of swelling. (d) TIVMI software interface showing the segmentation of newborn formation from femoral diaphysis at the prepathological state. (e) Three-dimensional (3D) reconstruction showing the periosteal reaction in transparency. The quantification of its volume can be calculated [Colour figure can be viewed at wileyonlinelibrary.com]

several fragments (comminuted nature), as well as the recent appearance of the callus (Figure 8b).

A CT scan of this femur was performed at the Department of Radiology of Moscow State University. The first examination of CT slices surprisingly revealed metallic artefacts embedded in the callus tissue, in close contact to the fragmented bones (Figure 8c). They are probably made of lead, as the material appears to be very dense and it is not fully penetrated by the X-rays. Slice-by-slice manual segmentation was performed, in order to separate remodelled bone (callus) from the bone fragments, stuck inside, based upon the difference of densities of the two tissues (Figure 8d). As the callus was recent, its lower density strongly contrasted with that of the bone fragments: this has facilitated the segmentation process. In addition, metallic artefacts were also individualized by segmentation. After the 3D reconstruction, the remodelled bone of the callus has been removed (Figure 8e and f), allowing us to visualize directly the bone fragments with sharp edges, which are seven in number, in addition to the two proximal and distal parts of the femur. It is therefore a comminuted fracture, a type of fracturing due to direct impact by a blunt or penetrating agent (Lovell, 1997). The global aspect of the fracture is corresponding to a direct trauma orientated from lateral to medial, with an upward direction.

Using 3ds Max software, we have reassembled the fragments together and corrected the angulation, in order to reconstruct the pretraumatic state of this femur (Figure 8g). This procedure brought two main additional information: (i) the 3D position of metallic fragments, which are concentrated in the area of the fracture, mostly present on its inner part, medially orientated, and (ii) the existence of an oval-shaped aperture located postero-laterally. These elements revealed the cause of the fracture: a wound by a lead bullet. A 3D reconstruction makes it possible to identify the location of the projectile's entrance hole and the location of the fractured site (figure 8h). These elements determine in forensic practice the ballistic characteristics of the shot. In our case, the direction of the shooting is oblique from bottom to top and from outside to inside. As femoral neck changes suggested a riding practice (Berthon et al., 2019; Pálfi & Dutour, 1996), our hypothesis is that the victim was a cavalier shot by an infantryman enemy. It is, to our knowledge, the first attempt of palaeo-ballistic reconstruction using 3D imaging in palaeopathology (Coqueugniot, Dutailly, Desbarats, Boulestin, et al., 2015) (supporting animation, Movie S1).

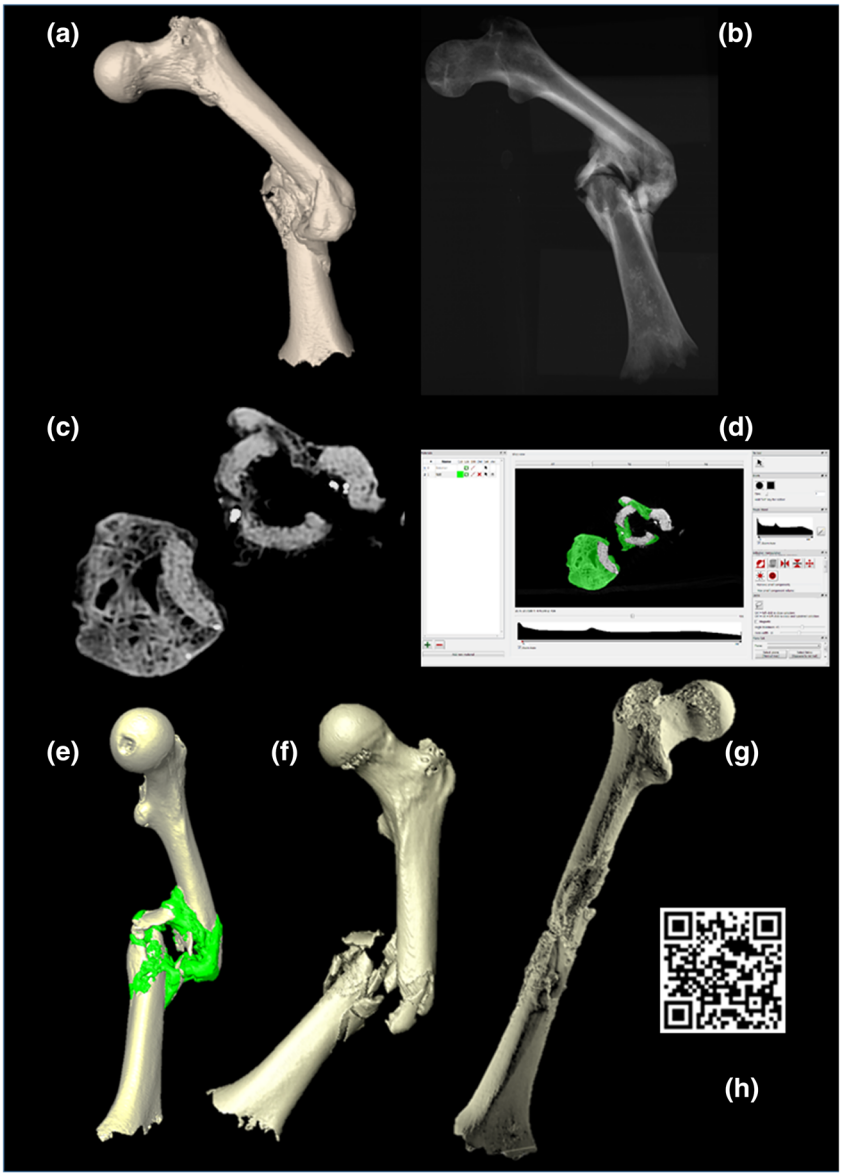

FIGURE 8 Comminuted femoral shaft fracture (Kaliningrad, Russian Federation, 1812). (a) Morphological aspect showing a partial healing in bad position. (b) Plain X-ray confirming the fracturing of the femoral diaphysis into several fragments. (c) Computed tomography (CT) scan, axial slice, revealing metallic artefacts embedded in the callus tissue. (d) TIVMI software interface showing the segmentation of callus tissue from cortical bone of femoral diaphysis. (e and f) Three-dimensional (3D) reconstructions showing the fracture area with and without callus tissue (green). (g) 3D reconstruction of the pretraumatic state. (h) QR code for video of the traumatic event reconstruction (palaeo-ballistic) [Colour figure can be viewed at wileyonlinelibrary.com]

3.1 | Respective contribution of 2D and 3D imaging to the palaeopathological diagnosis

We summarize in Table 2 the respective contribution of the three imaging methods (plain X-ray, CT slices, and 3D CT) to the diagnosis of these six palaeopathological cases and the added value of 3D.

4 | DISCUSSION

Palaeopathology benefited from CT since the 1980s (Wong, 1981), but the interest of 3D reconstruction from CT was mentioned 10 years later for palaeopathology (Pickering et al., 1990).

Since this moment, hundreds of papers joining the two keywords "palaeopathology" and "3D" were published, with a clear increasing in the last 3 years. However, most of these papers did not clearly mention the value of 3D as diagnostic method, and no one assessed its strengths and weaknesses for the retrospective diagnosis compared with that of conventional radiography and CT scans slices. Moreover, the legitimacy of 3D for palaeopathological diagnosis has been firmly challenged, and some authors argued against its use (Chhem, 2006; Chhem & Brothwell, 2008).

Our study is thus the first attempt, to our knowledge, to compare in a systematic way on a set of selected cases, the respective informative value of 2D and 3D radiological imaging methods for palaeopathological diagnosis, advocating the interest of multimodal approach. We showed that 3D imaging, in comparison with the input of 2D imaging, can bring an added value to the retrospective diagnosis, in at least three directions. Firstly, it reconstructs the volume surface of anatomical structures that are hardly visible on radiographs or CT slices: it allows then to better evidence some pathological changes. In our sample, this was of a great help for (i) showing lesions on brain surface and change diagnosis from a benign skull fracture to a traumatic brain injury (Case 1); (ii) evaluating the integrity of the spinal

TABLE 2 Respective contribution of plain radiography, 2D CT and 3D CT (surface extraction) to the palaeopathological diagnosis, with a highlight on added value of 3D imaging

Case number	Plain X-ray	CT slices	3D (surface extraction)	Added value of 3D
1	Taphonomic damages (crushing and missing parts). Benign healed fracture of frontal bone.	Angulation of a right juxta-coronal fragment of the frontal bone. Possible taphonomic origin.	Frontal bone depressed fracture with brain injury (TBI).	Evidence of TBI (X-rays diagnosed a benign fracture).
2	Thoracic angular kyphosis evoking a Pott disease.	No added value for diagnosis due to the strong angulation.	No significant narrowing of the spinal canal diameter.	The strong angular kyphosis did not narrow the spinal canal diameter.
3	Sacroiliac fusion. Rounded radiolucency adjacent to the fused zone.	Large cystic cavity overlapping the sacroiliac joint.	Presence of 2 mirror cysts on either side of the sacroiliac joint suggestive of tubercular sacroiliitis.	Evidence of 2 mirror cysts instead of one. Additional evidence for a diagnosis of tuberculosis.
4	Multiple rounded lytic lesions in favour of multiple myeloma or metastatic carcinoma.	Intradiploic multiple lesions with possible opening to intracranial or extracranial space.	Measurement of the neoplastic volume.	Unique opportunity of quantifying the neoplastic volume.
5	Localized periosteal reaction at middiaphysis with oval radiolucencies.	Antero-medial large new bone formation, moderate remodelling of the endosteal space suggesting gummatous osteoperiostitis evoking treponemal infection.	Visualization of the gummas, measurement of the new bone formation (7%) and reconstruction of prepathological state.	Reconstruction of the prepathological state.
6	Comminuted fracture in way of healing, complicated.	Comminuted bone fragments embedded in a recent callus, dense metallic artefacts.	Visualization of the traumatic state before healing (8 fragments). Reconstructions of the pretraumatic state, the trauma process by bullet and its (palaeo)ballistic.	Reconstruction of the pretraumatic and traumatic state. Ballistic reconstruction explaining the trauma.

TBI, traumatic brain injury.

canal involved by severe angular kyphosis due to spinal TB and then moderating the hypothesis of Pott's paraplegia (Case 2) and (iii) determining the relationships in space between the sacroiliac joint and the two cysts and then evidencing their mirror-like position and pus evacuation pathways in favour of TB infection (Case 3). Secondly, 3D imaging has the possibility to quantify pathological volumes, which was helpful for determining the evolutionary state of a neoplasia (Case 4). Finally, 3D imaging can reconstruct the prepathological state of a given part of the skeleton, allowing to follow virtually the past pathological processes: this represents a unique opportunity in palaeopathology (Coqueugniot, Dutailly, Desbarats, Buzhilova, et al., 2015). In our study, this approach was efficient for infectious process (Case 5) as well as for trauma (Case 6).

To sum up, we can affirm that 3D CT imaging, when using adequate methods of reconstruction, brings a real added value to the conventional 2D X-rays and underlines the interest of a multimodal approach, combining 2D and 3D imaging for the diagnosis in palaeopathology.

ACKNOWLEDGEMENTS

We thank the two anonymous reviewers for their helpful comments that allowed us to improve our manuscript. We are indebted to the colleagues who have entrusted us by making osteo-archaeological or fossil material available for this study. This research benefited from several funds: French-Russian Laboratory (CNRS/RAS) (LIA K1812, Anthropology and Archaeology of the Retreat of Russia, dir. O. Dutour and A. Buzhilova - French CNRS and Russian Academy of Sciences; Nouvelle-Aquitaine Regional Council (VIRTOS project); the Cluster of Excellence in Archaeological Sciences in Bordeaux (ANR-10-LABX-52).

CONFLICT OF INTEREST

None.

ORCID

Hélène Coqueugniot https://orcid.org/0000-0002-1844-4588
Olivier Dutour https://orcid.org/0000-0001-8134-788X

REFERENCES

Allam, A. H., Thompson, R. C., Wann, L. S., Miyamoto, M. I., & Thomas, G. S. (2009). Computed tomographic assessment of atherosclerosis in ancient Egyptian mummies. *JAMA*, *302*, 2091–2094.

Anonymous (1975). Chronique des fouilles effectuées en France en 1974 sur des sites médiévaux. *Archéologie Médiévale*, *5*, 515.

Appelboom, T., & Struyven, J. (1999). Medical imaging of the Peruvian mummy Rascar Capac. *The Lancet*, *354*, 2153–2155.

Aymard, I., Ardagna, Y., Lalys, L., Signoli, M., Gély, B., & Dutour, O. (2007). Etude anthropologique du site azilien des Iboussières (Malataverne, Drôme). In *Un siècle de construction du discours scientifique en préhistoire. 26e Congrès Préhistorique de France. Congrès du centenaire* (pp. 537–544). Avignon.

Baudouin, M. (1923). La radiographie appliquée à l'étude des lésions osseuses humaines préhistoriques. *Comptes Rendus de l'Académie Des Sciences*, *176*, 782–785.

Béclère, A. (1898). *Les Rayons de Röentgen et le diagnostic de la tuberculose*. Paris: Masson.

Belcastro, M. G., Mariotti, V., Bonfiglioli, B., Todero, A., Bocchini, G., Bettuzzi, M., … Morigi, M. P. (2014). Dental status and 3D reconstruction of the malocclusion of the famous singer Farinelli (1705–1782). *International Journal of Paleopathology*, *7*, 64–69.

Berthon, W., Tihanyi, B., Kis, L., Révész, L., Coqueugniot, H., Dutour, O., & Pálfi, G. (2019). Horse riding and the shape of the acetabulum: Insights from the bioarchaeological analysis of early Hungarian mounted archers (10th century). *International Journal of Osteoarchaeology*, *29*, 117–126.

Buikstra, J. (2019). *Ortner's identification of pathological conditions in human skeletal remains* (3rd ed.). Elsevier: San Diego, CA.

Buzhilova, A., Rigeade, C., Shvedchikova, T., Ardagna, Y., & Dutour, O. (2009). The discovery of a mass grave of Napoleon's great army in Kaliningrad (formerly Königsberg), Russian Federation: Preliminary results and interpretations. In L. Buchet, C. Rigeade, I. Séguy, & M. Signoli (Eds.), *9e journées d'Anthropologie de Valbonne* (pp. 375–383). Antibes, France: Editions ADPCA.

Cai, W.-L., & Hong, G.-B. (2018). Quantitative image analysis for evaluation of tumor response in clinical oncology. *Chronic Diseases and Translational Medicine*, *4*, 18–28.

Castro, M., Goycoolea, M., Galvez, M., Silva, V., Montoya, C., & Fuentes, J. (2019). Mastoid osteoma in a prehispanic cranium (1390 A.D.) from Northern Chile. *International Journal of Paleopathology*, *24*, 141–143.

Chamel, B., Coqueugniot, H., Dutour, O., Mindaoui, L., & Le Mort, F. (2017). Interpersonal violence or hunting accident among the last hunter-gatherers? A flint projectile embedded in a thoracic vertebra from the Early Neolithic site of Tell Mureybet, Syria. *Paléorient*, *43*, 25–34.

Chhem, R. K. (2006). Paleoradiology: Imaging disease in mummies and ancient skeletons. *Skeletal Radiology*, *35*, 803–804.

Chhem, R. K., & Brothwell, D. R. (2008). *Imaging mummies and fossils*. Berlin, Heidelberg: Springer.

Colardelle, R. (1996). Saint-Laurent et les cimetières de Grenoble du IVe au XVIIIe siècles. In H. Galinié, & E. Zadora-Rio (Eds.), *Archéologie du cimetière chrétien, Actes du 2e Colloque ARCHEA* (pp. 111–124). Orléans: 11e supplément à la Revue Archéologique du Centre de la France.

Conroy, G. C., & Vannier, M. W. (1985). Endocranial volume determination of matrix-filled fossil skulls using high-resolution computed tomography. In P. V. Tobias (Ed.), *Hominid evolution: Past, present and future* (pp. 419–426). New York: Alan R. Liss, Inc.

Coqueugniot, H., Dutailly, B., Desbarats, P., Buzhilova, A., & Dutour, O. (2015). Développement des virtothèques ostéologiques en anthropologie biologique et en paléopathologie. Application aux traumatismes de guerre de la période napoléonienne (Retraite de Russie, décembre 1812), première analyse virtuelle de paléo-balistique. In R. Vergnieux, & C. Delevoie (Eds.), *Actes du Colloque Virtual Retrospect 2013* (pp. 57–62). Pessac: Ausonius Publications.

Coqueugniot, H., Dutour, O., Arensburg, B., Duday, H., Vandermeersch, B., & Tillier, A. (2014). Earliest cranio-encephalic trauma from the Levantine Middle Palaeolithic: 3D reappraisal of the Qafzeh 11 Skull, consequences of pediatric brain damage on individual life condition and social care. Frayer D (ed). *PLoS ONE*, *9*, e102822.

Coqueugniot, H., Dutailly, B., Desbarats, P., Boulestin, B., Pap, I., Szikossy, I., … Dutour, O. (2015). Three-dimensional imaging of past skeletal TB: From lesion to process. *Tuberculosis*, *95*, S73–S79.

Coutinho Nogueira, D., Dutailly, B., Comte, F., Vasil'iev, A., Khokhlov, A., Shvedchikova, T., … Coqueugniot, H. (2019). "Gueule cassée" (facial injuries): A 3D paleotraumatology study and facial approximation of a Napoleonic soldier who died in 1812 at Königsberg during the Russian Campaign. *International Journal of Osteoarchaeology*, *29*, 191–197.

Dastugue, J. (1981). Pièces pathologiques de la nécropole moustérienne de Qafzeh. *Paléorient*, *7*, 135–140.

Dedekind, A. (1896). A novel use for the Roentgen rays. *British Journal of Photography*, *43*, 131.

Dufaÿ, B., & Gaultier, M. (2011). Premier bilan des fouilles archéologiques du prieuré de Saint-Cosme à La Riche près de Tours. *Bulletin de la Société archéologique de Touraine*, *62*, 83–104.

Dutailly, B., Coqueugniot, H., Desbarats, P., Gueorguieva, S., & Synave, R. (2009). 3D surface reconstruction using HMH algorithm. In *2009 16th IEEE International Conference on Image Processing (ICIP)*. IEEE: Cairo; 2505–2508.

Dutour, O., & Buzhilova, A. (2013). Paleopathological study of Napoleonic mass graves discovered in Russia. In C. J. Knüsel, & M. J. Smith (Eds.), *The Routledge handbook of the bioarchaeology of human conflict* (pp. 511–524). Abingdon and New York: Taylor and Francis Group.

Dutour, O., Gaultier, M., Dufaÿ, B., Dutailly, B., & Coqueugniot, H. (2013). Approche tridimensionnelle du myélome multiple en paléopathologie. In *Actes du colloque du Groupe des Paléopathologistes de Langue Française* (p. 10). Toulon: Centre archéologique du Var.

Dutour, O., Pálfi, G., Panuel, M., & Gély, B. (1995). Paleopathological study of Upper Palaeolithic remains from Southeastern France. *Journal of Paleopathology*, *7*, 98.

Flohr, S., Brinker, U., Schramm, A., Kierdorf, U., Staude, A., Piek, J., … Orschiedt, J. (2015). Flint arrowhead embedded in a human humerus from the Bronze Age site in the Tollense valley, Germany—A high-resolution micro-CT study to distinguish antemortem from perimortem projectile trauma to bone. *International Journal of Paleopathology*, *9*, 76–81.

Gaonkar, B., Macyszyn, L., Bilello, M., Sadaghiani, M. S., Akbari, H., Attiah, M. A., … Davatzikos, C. (2015). Automated tumor volumetry using computer-aided image segmentation. *Academic Radiology*, *22*, 653–661.

van der Gijp, A., van der Schaaf, M. F., van der Schaaf, I. C., Huige, J. C. B. M., Ravesloot, C. J., van Schaik, J. P. J., & ten Cate, T. J. (2014). Interpretation of radiological images: Towards a framework of knowledge and skills. *Advances in Health Sciences Education*, *19*, 565–580. https://doi.org/10.1007/s10459-013-9488-y

Gostner, P., Pernter, P., Bonatti, G., Graefen, A., & Zink, A. R. (2011). New radiological insights into the life and death of the Tyrolean Iceman. *Journal of Archaeological Science*, *38*, 3425–3431. https://doi.org/10.1016/j.jas.2011.08.003

Guyomarc'h, P., Santos, F., Dutailly, B., Desbarats, P., Bou, C., & Coqueugniot, H. (2012). Three-dimensional computer-assisted craniometrics: A comparison of the uncertainty in measurement induced by surface reconstruction performed by two computer programs. *Forensic Science International*, *219*, 221–227.

Pálfi, G., & Dutour, O. (1996). Activity-induced skeletal markers in historical anthropological material. *International Journal of Anthropology*, *11*, 41–55.

Hackett, C. J. (1976). *Diagnostic criteria of syphilis, yaws, and treponarid (treponematoses) and some other diseases in dry bones (for the use in osteo-archaeology)*. Berlin: Springer-Verlag.

Hernandez, M., & Hudson, M. J. (2015). Diagnosis and evaluation of causative factors for the presence of endemic treponemal disease in a Japanese sub-tropical island population from the Tokugawa period. *International Journal of Paleopathology*, *10*, 16–25.

Hervieu, P., Herrscher, E., & Colardelle, R. (2008). Discussion autour du statut de structures funéraires particulières: Le cas des caveaux de Saint-Laurent de Grenoble. *Socio-Anthropologie*, 55–74.

Jansen, R. J., Poulus, M., Taconis, W., & Stoker, J. (2002). High-resolution spiral computed tomography with multiplanar reformatting, 3D surface- and volume rendering: a non-destructive method to visualize ancient Egyptian mummi®cation techniques. *Computerized Medical Imaging and Graphics*, *6*, 211–216.

König, W. (1896). *14 Photographien mit Röntgen-Strahlen aufgenommen im physikalischen verein zu Frankfurt A.M.* Leipzig: Verlag von Johann Ambroius Barth.

Lewin, P. K., & Harwood-Nash, D. C. F. (1977). Computerized axial tomography in medical archeology. *Paleopathol. Newsl.*, 8–9.

Lovell, N. (1997). Trauma analysis in paleopathology. *Yearbook of Physical Anthropology*, *40*, 139–170.

Lynnerup, N. (2008). Computed tomography scanning and three-dimensional visualization of mummies and bog bodies. In R. Pinhasi, & S. Mays (Eds.), *Advances in human palaeopathology* (pp. 101–119). Chichester, UK: John Wiley & Sons, Ltd.

Marcsik, A., Szentgyorgyi, R., Gyetvai, A., Finnegan, M., & Pálfi, G. (1999). Probable Pott's paraplegia from the 7th–8th century A.D. In G. Pálfi, O. Dutour, J. Deák, & I. Hutás (Eds.), *Tuberculosis past and present* (pp. 333–339). Budapest, Szeged: Golden Book, Tuberculosis Foundation.

Marx, M., & D'Auria, S. H. (1988). Three-Dimensional CT reconstruction of an ancient human Egyptian mummy. *American Journal of Roentgenology*, *150*, 147–149.

Mays, S. (2008). Radiography and allied techniques in the palaeopathology of skeletal remains. In R. Pinhasi, & S. Mays (Eds.), *Advances in human palaeopathology* (pp. 77–100). Chichester, UK: John Wiley & Sons, Ltd.

Moodie, R. L. (1923). *Paleopathology: An introduction to the study of ancient evidences of disease*. Urbana, Illinois: University of Illinois Press.

Moodie, R. L. (1931). *Roentgenologic studies of Egyptian and Peruvian mummies*. Chicago: University of Chicago Press.

O'Brien, J. J., Battista, J. J., Romagnoli, C., & Chhem, R. K. (2009). CT imaging of human mummies: A critical review of the literature (1979–2005). *International Journal of Osteoarchaeology*, *19*, 90–98.

Pales, L. (1929). *État actuel de la Paléopathologie, contribution à l'étude de la pathologie comparative*. Bordeaux: Thèse de doctorat en médecine.

Panzer, S., Ketterl, S., Bicker, R., Schoske, S., & Nerlich, A. G. (2019). How to CT scan human mummies: Theoretical considerations and examples of use. *International Journal of Paleopathology*, *26*, 122–134.

Pernter, P., Gostner, P., Vigl, E. E., & Rühli, F. J. (2007). Radiologic proof for the Iceman's cause of death (ca. 5'300BP). *Journal of Archaeological Science*, *34*, 1784–1786.

Pickering, R. B., Conces, D. J., Braunstein, E. M., & Yurco, F. (1990). Three-dimensional computed tomography of the mummy Wenuhotep. *American Journal of Physical Anthropology*, *83*, 49–55.

Plischuk, M., De Feo, M. E., & Desántolo, B. (2018). Developmental dysplasia of the hip in female adult individual: Site Tres Cruces I, Salta, Argentina (Superior formative period, 400–1000 AD). *International Journal of Paleopathology*, *20*, 108–113.

Richards, G. D., Ojeda, H. M., Jabbour, R. S., Ibarra, C. L., & Horton, C. F. (2013). Bear phalanx traumatically introduced into a living human: Prehistoric evidence. *International Journal of Paleopathology*, *3*, 48–53.

Rothschild, B. M., Hershkovitz, I., & Dutour, O. (1998). Clues potentially distinguishing lytic lesions of multiple myeloma from those of metastatic carcinoma. *American Journal of Physical Anthropology*, *105*, 241–250.

Rowland, S. (1896). Preface. *Archives of Clinical Skiagraphy*, *1*, 3–4.

Ruffer, M. A. (1913). Studies in palæopathology in Egypt. *The Journal of Pathology and Bacteriology*, *18*, 149–162.

Ruffer, M. A. (1921). Pathological notes on the royal mummies of the Cairo museum. In R. L. Moodie (Ed.), *Studies in the paleopathology of Egypt* (pp. 166–178). Chicago: University of Chicago Press.

Shufeldt, R. W. (1893). Notes on paleopathology. *Popular Science Monthly*, *42*, 679–684.

Spoor, C. F., Zonneveld, F. W., & Macho, G. A. (1993). Linear measurements of cortical bone and dental enamel by computed tomography: Applications and problems. *American Journal of Physical Anthropology*, *91*, 469–484.

Thomson, J. (1896). The Rontgen rays. *Nature*, *53*, 581–583.

Tillier, A.-M. (1999). Les enfants moustériens de Qafzeh. In *Interprétation phylogénétique et paléoauxologique*. Paris: Cahiers de Paléoanthropologie. CNRS Editions.

Vandermeersch, B. (1981). *Les hommes fossiles de Qafzeh (Israël)*. Paris: Cahiers de Paléoanthropologie. CNRS Editions.

Wade, A. D., Beckett, R., Conlogue, G., Garvin, G., Saleem, S., Natale, G., … Nelson, A. (2019). Diagnosis by consensus: A case study in the importance of interdisciplinary interpretation of mummified remains. *International Journal of Paleopathology*, *24*, 144–153.

Weber, G. W. (2001). Virtual anthropology (VA): A call for Glasnost in paleoanthropology. *The Anatomical Record*, *265*, 193–201.

Wong, P. A. (1981). Computed tomography in paleopathology: Technique and case study. *American Journal of Physical Anthropology*, *55*, 101–110.

Woo, E. J., Lee, W.-J., Hu, K.-S., & Hwang, J. J. (2015). Paleopathological study of dwarfism-related skeletal dysplasia in a Late Joseon Dynasty (South Korean) population. Larsen CS (ed). *PLOS ONE*, *10*, e0140901.

Zuckerman, M. K., Garofalo, E. M., Frohlich, B., & Ortner, D. J. (2014). Anemia or scurvy: A pilot study on differential diagnosis of porous and hyperostotic lesions using differential cranial vault thickness in subadult humans. *International Journal of Paleopathology*, *5*, 27–33. https://doi.org/10.1016/j.ijpp.2014.02.001

SUPPORTING INFORMATION

Additional supporting information may be found online in the Supporting Information section at the end of this article.

How to cite this article: Coqueugniot H, Dutailly B, Dutour O. The third dimension in palaeopathology: How can three-dimensional imaging by computed tomography bring an added value to retrospective diagnosis? *Int J Osteoarchaeol*. 2020; 1–13. https://doi.org/10.1002/oa.2881